


Article

Visible Light-Driven SnIn₄S₈ Photocatalyst Decorated on Polyurethane-Impregnated Microfiber Non-Woven Fabric for Pollutant Degradation

Zhonghui Wang^{1,2}, Qiang Gao^{1,2}, Haihang Luo^{1,2}, Jianming Zhao^{1,2}, Haojun Fan^{1,2,*}, Yi Chen^{1,2} and Jun Xiang^{1,2} 

¹ Key Laboratory of Leather Chemistry and Engineering of Ministry of Education, Sichuan University, Chengdu 610065, China; wangzhonghui652@163.com (Z.W.); gaoqiang_scu@163.com (Q.G.); luohaihang0823@163.com (H.L.); jmzhao@achilleskunshan.com (J.Z.); chenyi_leon@scu.edu.cn (Y.C.); junxiang@scu.edu.cn (J.X.)

² National Engineering Research Center of Clean Technology in Leather Industry, Sichuan University, Chengdu 610065, China

* Correspondence: fanhaojun@scu.edu.cn

Abstract: In recent years, polyurethane has drawn great attention because of its many advantages in physical and chemical performance. In this work, firstly, polyurethane was impregnated in a non-woven fabric (NWF). Then, polyurethane-impregnated NWF was coagulated utilizing a wet phase inversion. Finally, after alkali treatment, microfiber non-woven fabrics with a porous polyurethane matrix (PNWF) were fabricated and used as substrates. SnIn₄S₈ (SIS) prepared by a microwave-assisted method was used as a photocatalyst and a novel SIS/PNWF substrate with multiple uses and highly efficient catalytic degradation ability under visible light was successfully fabricated. The surface morphology, chemical and crystal structures, optical performance, and wettability of SIS/PNWF substrates were observed. Subsequently, the photocatalytic performance of SIS/PNWF substrates was investigated by the decomposition of rhodamine B (RhB) under visible light irradiation. Compared with SIS/PNWF-2% (2%, the weight ratio of SIS and PNWF, same below), SIS/PNWF-5% as well as SIS/PNWF-15%, SIS/PNWF-10% substrates exhibited superior photocatalytic efficiency of 97% in 2 h. This may be due to the superior photocatalytic performance of SIS and the inherent hierarchical porous structure of PNWF substrates. Additionally, the hydrophobicity of SIS/PNWF substrates can enable them to float on the solution and further be applied on an open-water surface. Furthermore, tensile strength and recycle experiments demonstrated that SIS/PNWF substrates possessed superior mechanical strength and excellent recycle stability. This work provides a facile and efficient pathway to prepare SIS/PNWF substrates for the degradation of organic pollutants with enhanced catalytic efficiency.

Keywords: polyurethane; SnIn₄S₈; microfiber non-woven fabric; photocatalysis; degradation; recyclable



Citation: Wang, Z.; Gao, Q.; Luo, H.; Zhao, J.; Fan, H.; Chen, Y.; Xiang, J. Visible Light-Driven SnIn₄S₈ Photocatalyst Decorated on Polyurethane-Impregnated Microfiber Non-Woven Fabric for Pollutant Degradation. *Polymers* **2024**, *16*, 369. <https://doi.org/10.3390/polym16030369>

Academic Editor: Jeong In Han

Received: 21 December 2023

Revised: 25 January 2024

Accepted: 26 January 2024

Published: 29 January 2024



Copyright: © 2024 by the authors. Licensee MDPI, Basel, Switzerland. This article is an open access article distributed under the terms and conditions of the Creative Commons Attribution (CC BY) license (<https://creativecommons.org/licenses/by/4.0/>).

1. Introduction

Wastewater has attracted much more attention around the world in recent years due to its environmental and health risks [1,2]. Organic dyes, a type of significant pollutant, are widely applied in the textile, printing, paints, leather, cosmetics, paper industries, etc. [3,4]. Most dyes are very stable in the environment and difficult to be oxidated because of their complex aromatic structures [5,6]. Additionally, it has already demonstrated that dye wastewater prevents the penetration of visible light into the aqueous system, increases the biochemical oxygen demand (BOD) level, and inhibits the photosynthesis process of aquatic plants [7,8]. Organic dyes are toxic and even carcinogenic; when dyes wastewater

is directly discharged into water resources without proper treatment, it can present a serious threat to aquatic life and human health. Therefore, the dyes in wastewater must be removed before they are discharged into water resources. Given this, many technologies have been used to treat dye wastewater, including adsorption, membrane separation, ion exchange, filtration, electrochemical treatment, coagulation, and biological treatment [9,10]. However, these technologies have some drawbacks, such as a high operating cost, energy consumption, being sensitive to experimental conditions, low treatment efficiency, producing secondary pollution, etc. [11]. Therefore, it is very necessary to explore novel wastewater treatment technologies. Photocatalysis has been considered as one of the most effective and eco-friendly technologies because of its unique properties of degrading organic pollution through the utilization of solar energy, no secondary pollution, strong oxidation ability, sustainability, and simplicity of operation [12,13]. As is well known, the traditional semiconductor photocatalyst TiO_2 has been applied in the field of photocatalysis due to its low production cost, good chemical stability, excellent photocatalytic activity, and non-toxicity [14]. However, TiO_2 still has some drawbacks, such as a large band gap (around 3.2 eV), a small specific surface area, being prone to agglomeration, a weak photo-induced carriers separation ability, a difficulty in application to continuous flow systems, and a fast photo-induced electron–hole recombination rate, all of which hinder its practical application [15,16]. Fortunately, SnIn_4S_8 , a typical ternary metal sulfide compound with a narrow band gap (1.77–2.35 eV), strong visible-light absorption, and high stability, has occupied much concern and been applied in photocatalysis [17–19]. For instance, Wang and co-workers [20] fabricated hierarchical network-like SnIn_4S_8 microspheres via the low-temperature co-precipitation method, which exhibited the removal efficiency with a complete degradation of methyl orange within 40 min. Deng et al. [21] prepared g- $\text{C}_3\text{N}_4/\text{SnIn}_4\text{S}_8$ photocatalysts by the low-temperature co-precipitation method and these photocatalysts could rapidly degrade methyl orange under visible light. In Wang and co-workers' work [22], they employed the hydrothermal method to fabricate double-shell $\text{SnIn}_4\text{S}_8/\text{TiO}_2$ heterostructures and found that these hybrid photocatalysts displayed 90.08% degradation efficiency for methyl orange and 94.44% photoreduction efficiency for Cr (VI) within 60 min under visible light, respectively.

Up to the present, most photocatalysts have been powder-shaped materials, which are suspended in the treated wastewater. This will inevitably bring about some difficulties in recycling and reuse. On the one hand, they are not easily separated from the treated wastewater, which can result in secondary pollution to the environment [23–25]. Some methods have been used to separate the photocatalysts from the solution, including centrifugation, filtration, precipitation, etc. However, their separation operation procedures are complex and time-consuming. On the other hand, the aggregation and loss of powder-shaped materials in the recycling process could cause a decline in catalytic efficiency [26,27]. Furthermore, it is unsuitable for application in continuous flow systems [28]. Several approaches have been suggested to solve the disadvantages of powder-shaped photocatalysts in practical applications, including immobilization of powder-shaped photocatalyst in polymers, glass, ceramics, magnetic materials, etc. [29–31]. In Stoilova and co-workers' work [32], they incorporated TiO_2 into poly(methyl methacrylate) fibers by the electrospinning method and found that this type of composite could degrade methylene blue under ultraviolet light irradiation. Fu and co-workers [33] immobilized BiOI/rGO photocatalysts on Fe_3O_4 magnetic materials to fabricate $\text{BiOI}/\text{rGO}/\text{Fe}_3\text{O}_4$ hybrid photocatalysts. These photocatalysts could be rapidly separated from the reaction solution by an external magnet and showed 82.3% degradation efficiency for RhB after 10 cycles. In Zainal and co-workers' work [34], they immobilized TiO_2 -Chitosan photocatalysts on the glass and found that this type of hybrid photocatalysts could decompose methyl orange under a 15 W Philips white fluorescent light source. Recently, non-woven fabric (NWF) substrate has received widespread attention owing to its non-toxicity, good floatability, unique chemical inertness as well as its facile recovery [35]. These advantages make it a promising candidate for immobilizing powder-shaped materials, easier recovery, recycling, and reuse. Dao et al. [36]

fabricated a type of non-woven polyester fabric-supported Cu_2O /reduced graphene oxide nanocomposite; this photocatalyst exhibited 96% removal efficiency for methylene blue in 120 min. Huo et al. [37] assembled macroscopic D-g- C_3N_4 /sodium alginates/non-woven fabric by means of a two-step method of coating and cross-linking with CaCl_2 , which showed 94.3% degradation efficiency of RhB in 80 min and 97.8% degradation efficiency of tetracycline hydrochloride in 60 min under visible light irradiation, respectively. Meanwhile, this type of non-woven fabric photocatalysts could be easily recycled and retains excellent stability in the photocatalytic reaction.

Up to now, polyurethane has received a lot of attention due to its ascendant mechanical performance, favorable abrasion resistance, and superior flexibility [38,39]. In view of this, to improve the elasticity and tensile strength of non-woven fabrics, polyurethane with repeating carbamate groups ($-\text{NHCOO}-$) was impregnated in the fibers. Subsequently, polyurethane-impregnated non-woven fabric was coagulated by means of a wet phase inversion. Finally, after alkali treatment, microfiber non-woven fabric with a porous polyurethane matrix (PNWF) was fabricated. On account of its three-dimensional structure, high porosity, good mechanical intensity as well as its laudable chemical resistance, microfiber non-woven fabric has been widely applied in synthetic leather, wear, electromagnetic shielding, etc. [40–43]. However, there have been few reports on its applications in photocatalysis.

Recently, a microwave-assisted method has been widely used due to its unique characteristics of fast heating speed, high yields, high purity of the products, and homogenous dielectric heating [44,45]. Compared with the conventional hydrothermal method, the microwave-assisted method can shorten the reaction time from several hours to a few minutes or even seconds. Chumha et al. [46] prepared CuInS_2 nanoparticles by the microwave heating process with a 7.5 min reaction time and discovered that this photocatalysts could degrade methylene blue and rhodamine B with 91.21% and 97.8% degradation efficiency within 360 min under visible light irradiation, respectively. Li and co-workers [47] synthesized Fe_3O_4 /rGO composites by the microwave synthesis method. They found the size and morphology of nanocomposites could be tuned by changing the microwave reaction time. Therefore, the microwave-assisted method is expected to rapidly prepare photocatalysts and further contribute to improving the efficiency of the dye wastewater treatment.

In this work, in order to solve the disadvantages of powder-shaped photocatalysts in recycling and reuse, SIS/PNWF substrates were firstly fabricated and applied in the field of photocatalysis. First of all, SIS was synthesized by the means of a microwave-assisted method according to our previous report [48], and deposited on the PNWF substrates to assemble the SIS/PNWF substrates. Subsequently, the surface morphology, structure and optical performance of as-prepared SIS and a series of SIS/PNWF substrates were observed by scanning electron microscope, X-ray photoelectron spectroscopy, X-ray diffraction instruments, attenuated total reflection-Fourier transform infrared spectrometer, and UV-Vis-NIR diffuse reflectance spectrophotometer, respectively. The hydrophobicity of SIS/PNWF substrates can allow them to float on the solution and be applied in an open water surface. In addition, the photocatalytic performance of SIS/PNWF substrates was investigated by the decomposition of RhB under visible light irradiation. The tensile strength and recycle experiments demonstrated that SIS/PNWF substrates possessed superior mechanical strength and excellent recycle stability. Especially, after each photocatalytic reaction, the spent SIS/PNWF substrates were easily recovered from the reaction system by a nipper, which solved the disadvantages of powder-shaped photocatalysts in recycling and reuse. Thus, this work provides a facile and efficient pathway to prepare SIS/PNWF substrates for the degradation of organic pollutants.

2. Experiment

2.1. Materials

Thioacetamide (TAA, 99.0%), sodium dodecyl benzene sulfonate (SDBS), tin chloride pentahydrate ($\text{SnCl}_4 \cdot 5\text{H}_2\text{O}$, 99.9%), ammonium sulfate ($(\text{NH}_4)_2\text{SO}_4$), and indium chloride

tetrahydrate ($\text{InCl}_3 \cdot 4\text{H}_2\text{O}$, 99.9%) were obtained from Aladdin Chemical Reagent Co., Ltd. (Shanghai, China). Ethanol and sodium hydroxide (NaOH) were acquired from the Kelong Chemical Incorporated Co. Ltd., Chengdu, China. Waterborne polyurethane was prepared according to our previous work [49]. All reagents were used without any further purification. The sea-island bicomponent non-woven fabric compositing with polyamide-6 (PA6) and polyethylene terephthalate (PET) was obtained from the Zhejiang Meisheng Industrial Co., Ltd. (Shaoxing, China).

2.2. Fabrication of Three-Dimensional Microfiber Non-Woven Fabric

First, the sea-island bicomponent NWF was dipped in waterborne polyurethane with 25 wt% solid content. Waterborne polyurethane was utterly and uniformly penetrated into the NWF by pressing and squeezing with a round iron bar. Then, polyurethane-impregnated NWF was coagulated by being submerged into the ammonium sulfate solution (3 wt%) at pH 2–3 for 25 min. Subsequently, the aforementioned NWF was immersed in the 10 wt% NaOH solution at 90 °C for 90 min to remove PET. After washing and drying, the three-dimensional PNWF substrates with high porosity were fabricated.

2.3. Preparation of SnIn_4S_8 Photocatalysts

According to our previous report [48], SIS was synthesized via the microwave-assisted method. First of all, 0.6 mmol $\text{InCl}_3 \cdot 4\text{H}_2\text{O}$, 0.15 mmol $\text{SnCl}_4 \cdot 5\text{H}_2\text{O}$, 1.89 mmol SDBS, and 1.2 mmol TAA were dispersed in 50 mL anhydrous ethanol and continuous stirring was applied for 40 min at room temperature. Subsequently, the above-mentioned mixture was transferred to the microwave teflon vessel with an automatic application of microwave power output (0 to 950 W) and temperature sensor. Then, the microwave unit was heated at 180 °C for 20 min. After the reaction, the microwave reaction vessel was cooled down using compressed air. Finally, the yellow product was obtained and washed with deionized water and ethanol three times and freeze-dried for further use.

2.4. Preparation of SIS/PNWF Substrates

Firstly, a certain quantity of SnIn_4S_8 photocatalysts was dispersed in 50 mL deionized water. The PNWF substrate was cut into a size of 4 cm × 4 cm, was then immersed into the as-prepared SIS suspension, and shaken for 2 h at room temperature. The obtained SIS/PNWF substrates were washed in deionized water three times and then dried in an oven at 70 °C for 8 h. SIS/PNWF substrates were defined as SIS/PNWF-2% (2%, the weight ratio of SIS and PNWF, same below), SIS/PNWF-5%, SIS/PNWF-10%, and SIS/PNWF-15%.

2.5. Evaluation of Photocatalytic Activity

The photocatalytic activities of a series of SIS/PNWF substrates were evaluated by degradation of RhB. A 300 W xenon lamp (CEL-HXF300, China Education Au-light company, Beijing, China) coupled with an optical cutoff filter of 400 nm was utilized as a visible light source. The distance between the light source and the sample was 10 cm. A series of SIS/PNWF substrates were immersed in 50 mL solution with 30 mg/L RhB, respectively. The aforementioned suspension was constantly stirred in the dark for 2 h to achieve an adsorption–desorption equilibrium. Then the suspension with SIS/PNWF substrates was exposed to a 300 W xenon lamp under constant stirring conditions. Subsequently, approximately 3 mL of aliquot was collected at different times and immediately filtered through a 0.45 μm filter membrane. The absorbance of the RhB was analyzed by a UV-Vis spectrophotometer with a scan speed of 600 $\text{nm} \cdot \text{min}^{-1}$ at 556 nm (3900H, Hitachi, Tokyo, Japan). The following equation was used to evaluate the RhB removal efficiency:

RhB removal efficiency (RE) = $(A_0 - A_t)/A_0 \times 100\%$, where A_0 represents the initial absorbance of RhB, and A_t denotes the absorbance of RhB at a certain reaction time t min.

2.6. Characterization

Surface morphologies of as-prepared SIS, NWF, PNWF, and SIS/PNWF-10% substrates were surveyed via a Cambridge CamScanCS3400 field emission scanning electron microscope (SEM). X-ray photoelectron spectroscopy (XPS) analysis of the SIS/PNWF-10% substrate was conducted on a Kratos XSAM800 system with an Al K α . The crystal phases of SIS and SIS/PNWF substrates were observed by an X-ray diffraction (XRD) instrument (Kratos, AXIS Ultra DLD) using CuK α radiation in the two theta ranging from 10° to 80°. UV-Vis-NIR diffuse reflectance spectra of SIS and a series of SIS/PNWF substrates were performed on a PE1050+ spectrophotometer with an integrating sphere (PerkinElmer, Waltham, MA, USA) ranging from 200 to 700 nm at room temperature. Barium sulfate was used as a reference in the testing experiment. The absorbance of the RhB solution was measured by a UV-Vis spectrophotometer (3900H, Hitachi, Japan) with the scan rate of 600 nm·min⁻¹ at 556 nm. Attenuated total reflection-Fourier transform infrared (ATR-FTIR) spectra of the as-prepared samples were measured by a spectrum 3 FTIR spectrometer (PerkinElmer, USA) in a wavenumber range from 650 to 4000 cm⁻¹ at 2 cm⁻¹ resolution. The water contact angles of NWF, PNWF, SIS/PNWF-10% substrates were measured by an optical contact angle goniometer (DSA30s, KRUSS, Hamburg, Germany) with an automatic controller and a high-speed camera using 3 μ L water drops at room temperature. The tensile strength of as-prepared SIS/PNWF substrates was determined on an electronic universal testing machine (AI-7000 SN, Gotech Testing Machines Co., Ltd., Dongguan, China) equipped with a 100 N load cell with a tensile speed of 100 mm·min⁻¹ at room temperature. The average thickness of each sample was measured by a GT-313-A pachymeter (Gotech Testing Machines, China) at room temperature. Every as-prepared sample was measured three times to calculate their average value and standard deviation.

2.7. Regeneration and Reuse of SIS/PNWF Substrates

After each photocatalytic reaction, the spent SIS/PNWF substrates were easily recovered from the reaction system by a nipper, then washed with 100 mL DI water three times and dried at 60 °C for 8 h. The regenerated SIS/PNWF substrates were reused for the decomposition of RhB under the same reaction conditions as with the fresh SIS/PNWF substrates.

3. Results and Discussion

3.1. Morphology

The surface morphologies of as-prepared SIS, NWF, PNWF and SIS/PNWF-10% substrates were observed by SEM. The pure SIS displays noticeable 3D hierarchical urchin-like microspheres with an average diameter of approximately 1–2 μ m (Figure 1(a₁)). The high magnification SEM image (Figure 1(a₂)) further demonstrates that the urchin-like microspheres are fabricated by in situ self-assembly of the 2D disordered nanosheets, which is consistent with our previous work [48].

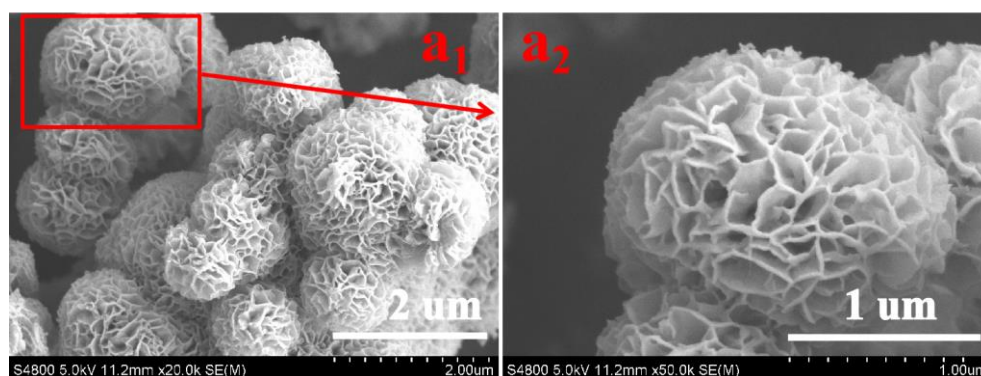


Figure 1. The low-magnification (a₁) and high-magnification (a₂) SEM images of SIS.

The SEM images of NWF, PNWF and SIS/PNWF-10% substrates are illustrated in Figure 2, respectively. For the NWF, it reveals that the average diameter of the single sea–island fiber is about 20 μm (Figure 2(a₁,a₂)). Figure 2(b₁,b₂) indicates that the individual island fiber is separated into many microfibrils with a diameter of approximately 2–3 μm , which is clearly lower than that of the single sea–island fiber for the NWF. Further observation reveals that there are plentiful voids in the PNWF substrate, which can favor increasing the specific surface area of the substrates. As depicted in Figure 2(c₁,c₂), SIS microspheres are densely distributed on the surface of PNWF substrates. These results show that SIS/PNWF substrates were successfully fabricated.

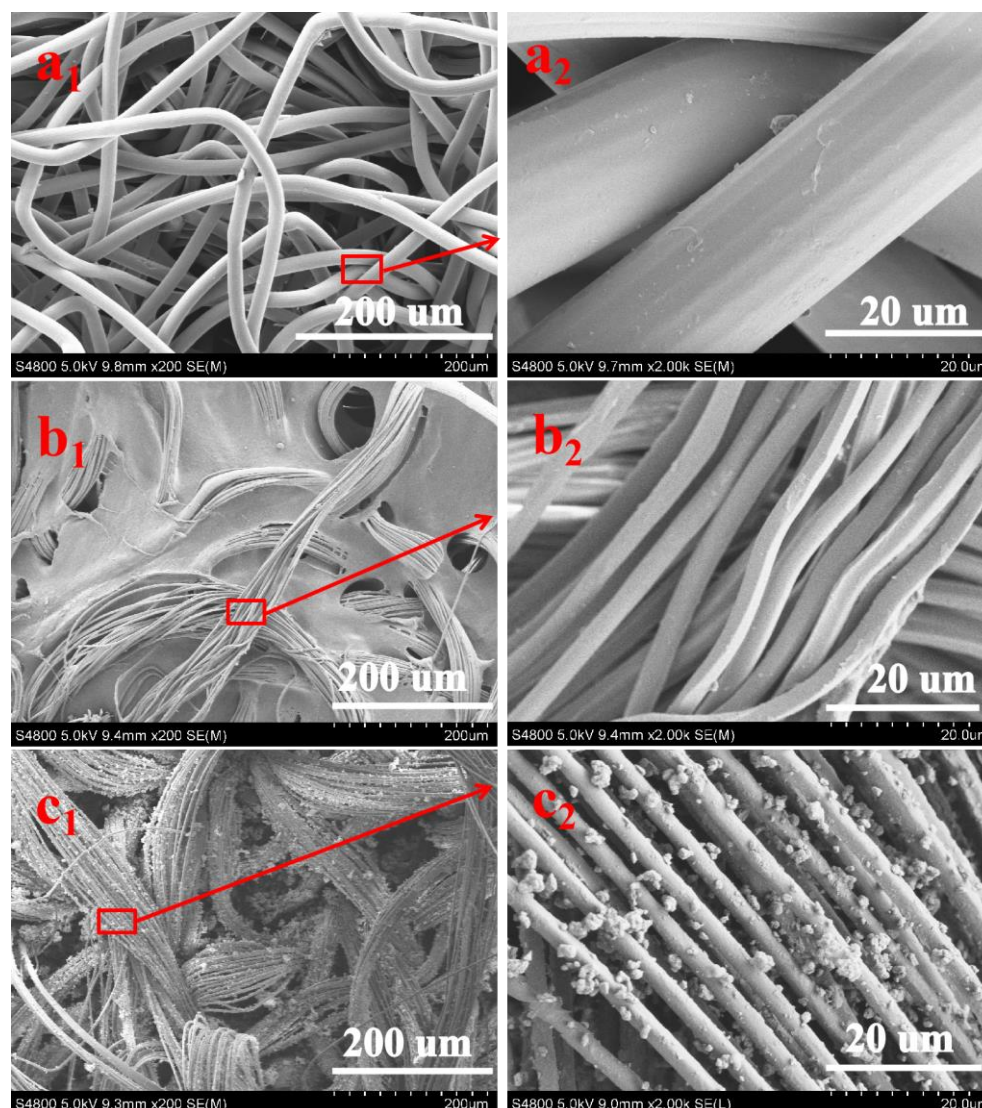


Figure 2. The SEM images of NWF (a₁,a₂), PNWF (b₁,b₂) and SIS/PNWF-10% substrates (c₁,c₂).

3.2. Crystal Structure

The XRD patterns of as-prepared SIS, PNWF, and SIS/PNWF substrates are presented in Figure 3. The five main characteristic diffraction peaks at 18.5°, 27.4°, 28.9°, 48.0°, and 49.8° can be readily ascribed to the (202), (311), (222), (440), (531) crystalline planes of the cubic phase of SnIn₄S₈, respectively. The peaks at two theta values of 20.8° and 23.8° correspond to the (200) and (002) crystalline planes of polyamide-6. Interestingly, the diffraction peaks of SIS at two thetas of 27.4°, 28.9°, 48.0° and 49.8° can be observed on the SIS/PNWF substrates. These results further demonstrate that SIS was successfully

deposited on the surface of PNWF substrates, and the structures of the SIS and PNWF had no significant influence on the hybridization process.

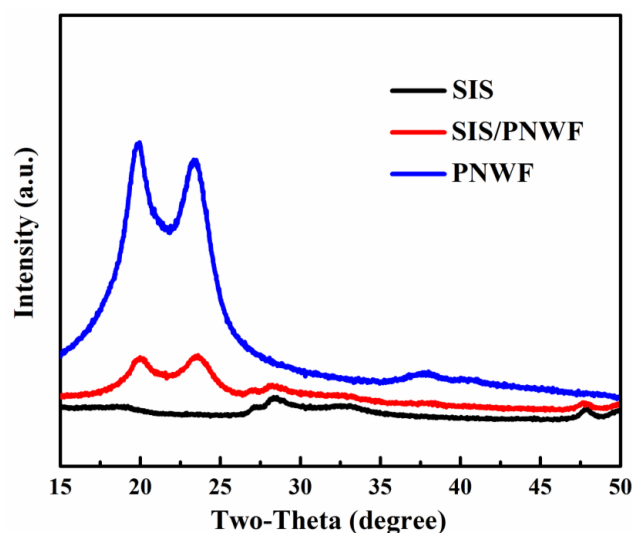


Figure 3. The XRD patterns of SIS, SIS/PNWF-10%, and PNWF substrates.

3.3. XPS Analysis

XPS was employed to investigate the element's composition and the chemical state of the SIS/PNWF-10% substrate. A survey spectrum clearly shows that the Sn, In, and S elements existed in the SIS/PNWF substrate (Figure 4a). The intense peaks located at 444.9 eV and 452.4 eV (Figure 4b) are attributed to In 3d_{5/2} and In 3d_{3/2} of In³⁺, respectively. As exhibited in Figure 4c, the obvious peaks of 486.4 eV and 494.8 eV can be assigned to the Sn 3d_{5/2} and Sn 3d_{3/2}, respectively. This result demonstrates that Sn⁴⁺ exists in the SIS/PNWF substrate. As for the S 2p spectrum (Figure 4d), two apparent peaks at 161.4 eV and 162.6 eV can be assigned to the S 2p_{1/2} and S 2p_{3/2} of S²⁻, respectively. In other words, the above results further confirm the formation of SIS/PNWF substrates.

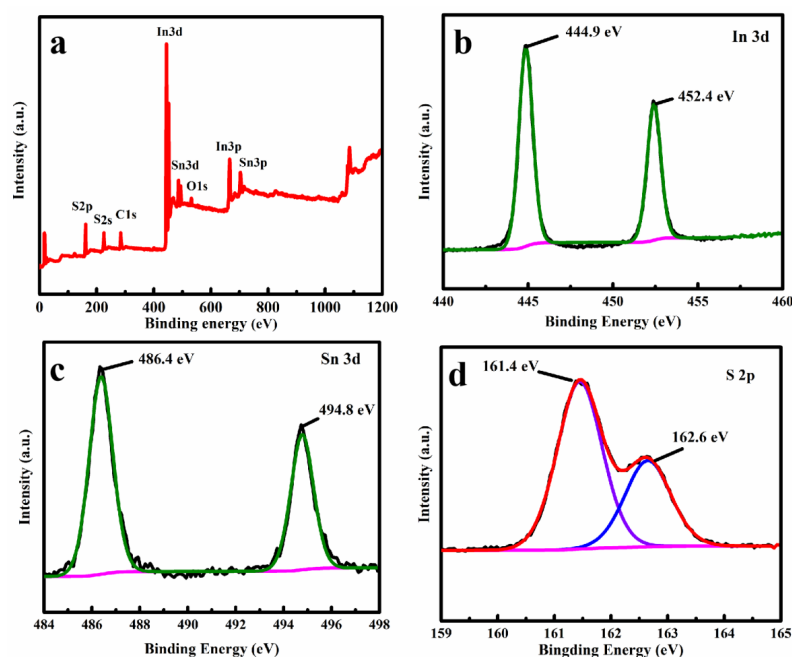


Figure 4. The XPS survey spectrum (a) and In 3d (b), Sn 3d (c), S 2P (d) spectra of SIS/PNWF-10% substrate.

3.4. UV-Vis Diffuse Reflectance Spectra

The optical absorption properties of the PNWF and a series of SIS/PNWF were determined by UV-Vis diffuse reflectance spectrometer with a wavelength ranging from 200 to 780 nm at room temperature. As denoted in Figure 5, PNWF substrates display no obvious absorption at a wavelength greater than 320 nm. After SIS was deposited on the surface of the PNWF, the absorption intensities of the SIS/PNWF in the visible light region distinctly increased, which can be ascribed to the strong absorption of SIS in the visible region. Furthermore, the absorption edges of the SIS/PNWF substrates are apparently red-shifted with the increase in SIS photocatalyst contents. These features suggested that the SIS photocatalysts endowed the PNWF with a conspicuous visible-light responsive performance.

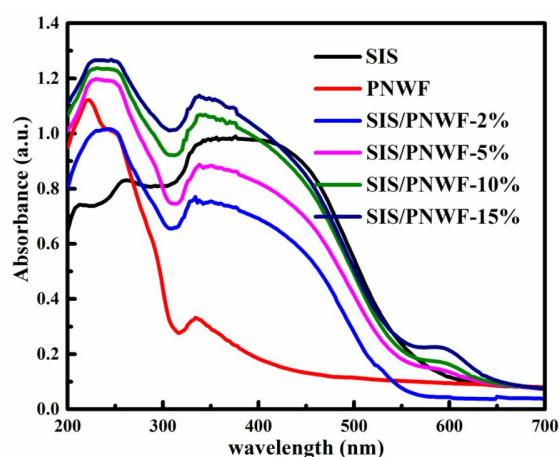


Figure 5. The UV-vis diffuse reflectance spectra of SIS, PNWF, SIS/PNWF-2%, SIS/PNWF-5%, SIS/PNWF-10%, and SIS/PNWF-15% substrates.

3.5. FT-IR Spectra

ATR-FTIR spectroscopy was applied to survey the surface chemical structure change in PNWF and SIS/PNWF-10% substrates. As illustrated in Figure 6, the characteristic peaks are at 3304, 1645, and 1540 cm^{-1} , which is consistent with $\nu_{\text{N-H}}$, $\nu_{\text{C=O}}$ and the combining absorption of both $\delta_{\text{N-H}}$ and $\nu_{\text{C-N}}$, respectively. The prominent peaks at 2950 and 2830 cm^{-1} correspond to the C-H stretching vibration for $-\text{CH}_3$. Further observation reveals that the spectrum of the PNWF is akin to that of the SIS/PNWF substrate. Therefore, the FT-IR spectrum indicates that the structure of the PNWF is not affected by the incorporation procedure of SIS.

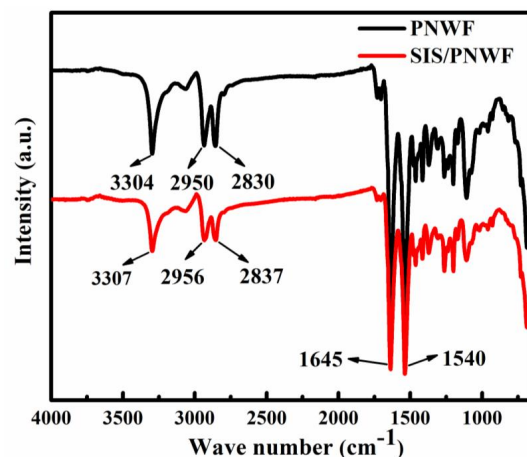


Figure 6. FTIR spectra of PNWF and SIS/PNWF-10% substrates.

3.6. Wettability

Wettability is the crucial factor affecting the practical application. In order to compare the difference in the wettability of as-prepared samples, the water contact angles of NWF, PNWF and SIS/PNWF-10% substrates were measured with a contact angle goniometer with an automatic controller and a high-speed camera. In this experiment, the water drops can rapidly spread and wet the NWF substrate, while water drops on the PNWF and SIS/PNWF-10% substrates can remain on the substrates surface for a while. As presented in Figure 7, the water contact angles of the PNWF and SIS/PNWF-10% substrates are 94° and 125° , respectively. This result demonstrates that SIS loading can change the wettability of the PNWF substrate surface. It can be explained that hierarchical urchin-like microspheres composed of the disordered nanosheets can trap a lot of air in their pores, resulting in a certain hydrophobicity of the SIS/PNWF-10% substrate [50]. On account of this hydrophobic performance, the SIS/PNWF-10% substrate can also be applied in wastewater treatment on an open surface such as a lake.

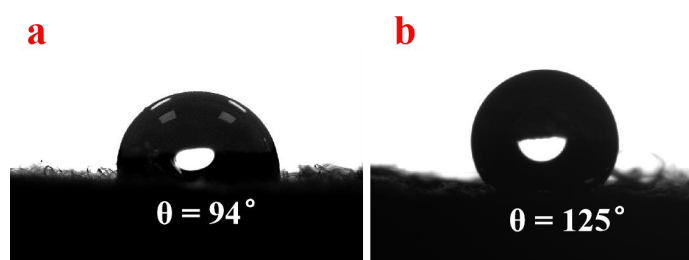


Figure 7. The water contact angles of PNWF (a), SIS/PNWF-10% (b) substrates.

3.7. Photocatalytic Properties of SIS/PNWF Substrates

The photocatalytic activity for RhB over a series of SIS/PNWF substrates was estimated under visible light. Compared with the PNWF, the SIS/PNWF substrates show enhanced photocatalytic performance (Figure 8). Just as was predicted, the photocatalytic activity of the SIS/PNWF substrates is clearly affected by the SIS content. It is clear that the RhB degradation rate gradually rises from 81.2% to 97% when the SIS photocatalysts content increases from 2% to 10%, whereas the degradation efficiency of RhB descends when the dosage ratio of SIS photocatalysts further increases to 15%. It can be inferred that an excess of photocatalysts could increase light scattering and bring down the absorbance, resulting in a decline in the degradation rate of the contaminants [51]. Therefore, the photocatalytic activity of a series of as-prepared SIS/PNWF substrates first increased and then reduced with an increase in the SIS content, indicating that the optimized weight ratio of SIS to PNWF was 10%. The enhanced photocatalytic activity of the SIS/PNWF-10% substrate should be attributed to the successful loading of SIS, the strong light absorption, and the inherent hierarchical porous structure of the PNWF substrate.

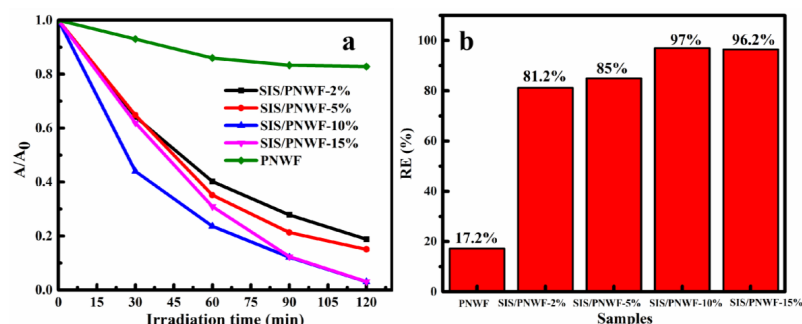


Figure 8. Photocatalytic activity (a) and photocatalytic degradation efficiency (b) of PNWF, SIS/PNWF-2%, SIS/PNWF-5%, SIS/PNWF-10%, and SIS/PNWF-15% substrates for RhB under visible light irradiation.

3.8. Reusability and Stability of the SIS/PNWF Substrates

Generally, the reusability and stability of photocatalysts are key factors affecting their practical application. In this work, the reusability and stability of SIS/PNWF substrates were studied. After each photocatalytic reaction, the SIS/PNWF substrate was pulled out from the reaction system by a nipper, then washed with DI water several times and dried at 60 °C for 8 h. As shown in Figure 9, the removal rate of RhB can reach up to 97% within 2 h under a visible light irradiation. After running four cycles, the degradation rate of RhB can still maintain 84%. The results indicate that SIS/PNWF substrates have good recyclability and stability. A slight decrease in the photocatalytic activity of the recovered SIS/PNWF substrates may be explained by the fact that a small amount of SIS photocatalyst could be lost in the process of consecutive recycling experiments.

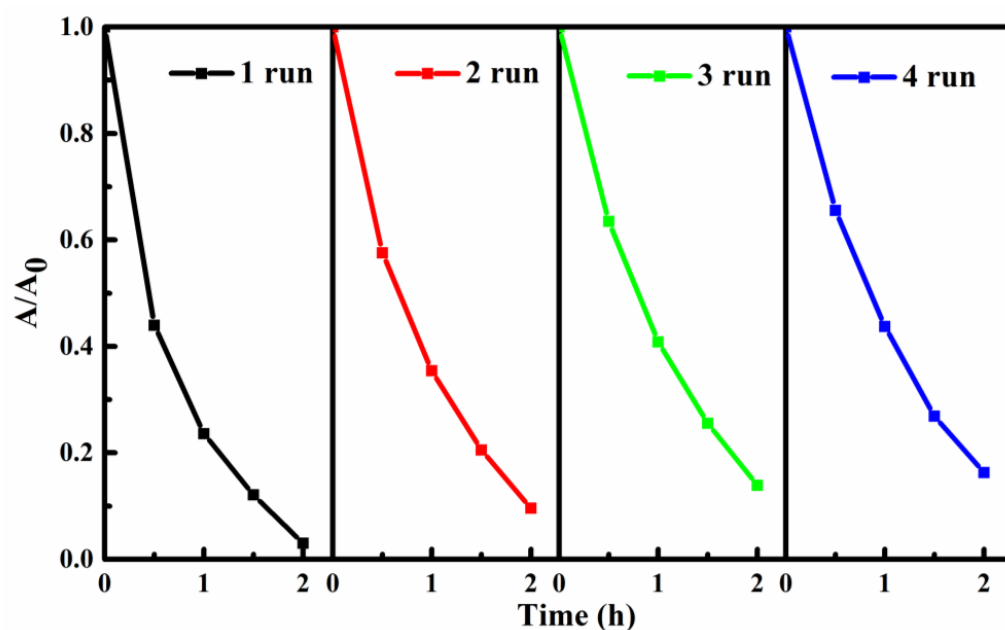


Figure 9. Photodegradation reusability of RhB over SIS/PNWF-10% substrate.

3.9. Tensile Strength of the SIS/PNWF Substrates

Mechanical performance is the key factor affecting the stability of the materials [52]. The tensile strength of the NWF, PNWF, SIS/PNWF-10%, and SIS/PNWF-10% (used four times) substrates was evaluated by an electronic universal testing machine with the tensile speed of 100 mm·min⁻¹ at room temperature. As depicted in Figure 10, the tensile strength of the PNWF substrate with the value of 10 MPa is greater than that of the NWF substrate, which indicates that polyurethane is beneficial for improving the tensile strength of the PNWF substrate. Interestingly, after depositing SIS photocatalysts on the PNWF substrate, the SIS/PNWF-10% substrate showed enhanced tensile strength with a value of 12.4 MPa. This result can be interpreted as indicating that SIS photocatalysts are conducive to enhancing the tensile strength of the PNWF substrate. Moreover, after running four cycles, the SIS/PNWF-10% substrate still maintains excellent tensile strength with the value of 12.3 MPa. Thus, these results indicate that the SIS/PNWF-10% substrate possesses superior tensile strength.

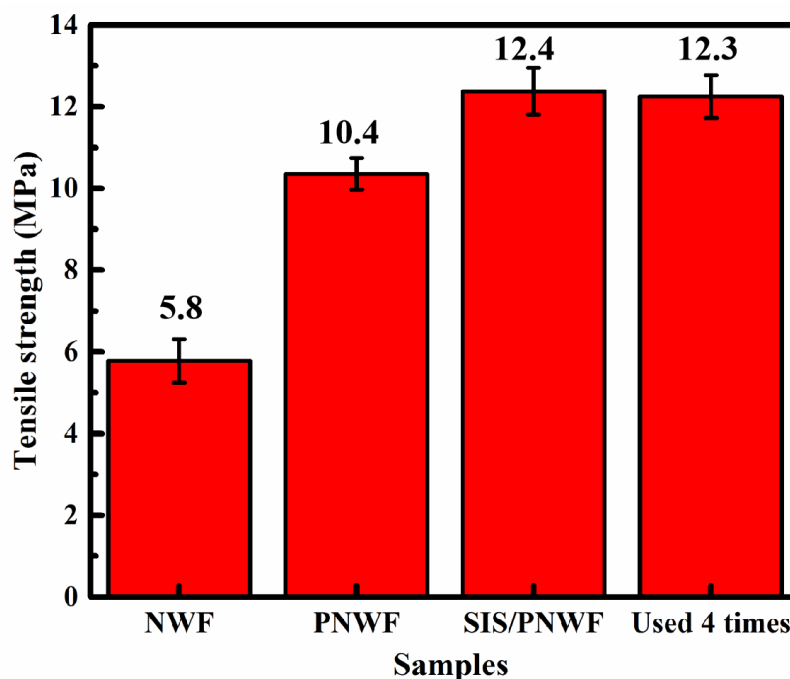


Figure 10. Tensile strength of NWF, PNWF, SIS/PNWF-10%, and SIS/PNWF-10% substrate used 4 times.

4. Conclusions

In summary, microfiber non-woven fabrics with a porous polyurethane matrix were fabricated by impregnated polyurethane, coagulation, and alkali treatment procedures. SIS was prepared by a facile microwave-assisted method and deposited on polyurethane-impregnated NWF substrates. The optimal SIS/PNWF-10% substrate displayed enhanced photocatalytic activity with a 97% degradation rate to RhB within 2 h under visible light irradiation. The enhanced photocatalytic activity of the SIS/PNWF-10% substrate should be attributed to the successful loading of SIS, the strong light absorption, and an inherent hierarchical porous structure of the PNWF substrates. Additionally, the SIS/PNWF-10% substrate showed excellent reusability and stability, and superior tensile strength. The hydrophobicity of the SIS/PNWF substrates could enable them to float on the solution and be applied on an open-water surface. This work provides a facile and efficient pathway to prepare SIS/PNWF substrates for the degradation of organic pollutants.

Author Contributions: Z.W.: Investigation, Methodology, Data curation, Writing—original draft, Writing—review and editing. Q.G.: Data curation. H.L.: Data curation. J.Z.: Data curation. H.F.: Supervision, Project administration, Writing—review and editing. Y.C.: Data curation, Visualization, Investigation. J.X.: Data curation, Analysis, Visualization, Supervision. All authors have read and agreed to the published version of the manuscript.

Funding: The authors would like to acknowledge the financial support for this work from the Opening Project of the Key Laboratory of Leather Chemistry and Engineering (Sichuan University), the Ministry of Education and the Synthetic Leather and High-Performance Fibers Innovation Team (2020SCUNG122).

Institutional Review Board Statement: Not applicable.

Data Availability Statement: The data presented in this study are available on request from the corresponding author.

Conflicts of Interest: The authors declare that they have no known competing financial interests or personal relationships that could have appeared to influence the work reported in this paper.

References

1. Wang, W.; Niu, Q.; Zeng, G.; Zhang, C.; Huang, D. Applied Catalysis B: Environmental 1D Porous Tubular g-C₃N₄ Capture Black Phosphorus Quantum Dots as 1D/0D Metal-Free Photocatalysts for Oxytetracycline Hydrochloride Degradation and Hexavalent Chromium Reduction. *Appl. Catal. B Environ.* **2020**, *273*, 119051. [[CrossRef](#)]
2. Bao, H.; Wu, M.; Meng, X.; Han, H.; Zhang, C.; Sun, W. Application of electrochemical oxidation technology in treating high-salinity organic ammonia-nitrogen wastewater. *J. Environ. Chem. Eng.* **2023**, *11*, 110608. [[CrossRef](#)]
3. Song, Y.; Wang, L.; Qiang, X.; Gu, W.; Mang, Z.; Wang, G. An overview of biological mechanisms and strategies for treating wastewater from printing and dyeing processes. *J. Water Process Eng.* **2023**, *55*, 104242. [[CrossRef](#)]
4. Modroga, C.; Căprărescu, S.; Dăncilă, A.M.; Orbuleț, O.D.; Grumezescu, A.M.; Purcar, V.; Radițoiu, V.; Fierascu, R.C. Modified Composite Based on Magnetite and Polyvinyl Alcohol: Synthesis, Characterization, and Degradation Studies of the Methyl Orange Dye from Synthetic Wastewater. *Polymers* **2021**, *13*, 3911. [[CrossRef](#)]
5. Wei, J.; Yuan, M.; Wang, S.; Wang, X.; An, N.; Lv, G.; Wu, L. Recent advances in metal organic frameworks for the catalytic degradation of organic pollutants. *Collagen Leather* **2023**, *5*, 33. [[CrossRef](#)]
6. Anisuzzaman, S.; Joseph, C.; Pang, C.; Affandi, N.; Maruja, S.; Vijayan, V. Current Trends in the Utilization of Photolysis and Photocatalysis Treatment Processes for the Remediation of Dye Wastewater: A Short Review. *ChemEngineering* **2022**, *6*, 58. [[CrossRef](#)]
7. Moyo, S.; Makhanya, B.; Zwane, P. Use of bacterial isolates in the treatment of textile dye wastewater: A review. *Heliyon* **2022**, *8*, e09632. [[CrossRef](#)]
8. Alharthi, F.A.; Albaeejan, M.A.; Alshayiqi, A.A.; Aldubeikl, H.K.; Hasan, I. Enhanced visible-light-driven photocatalytic degradation of azo dyes by heteroatom-doped nickel tungstate nanoparticles. *Nanotechnol. Rev.* **2023**, *12*, 20230143. [[CrossRef](#)]
9. Han, C.; Cheng, C.; Liu, F.; Li, X.L.; Wang, G.; Li, J. Preparation of CdS–Ag₂S nanocomposites by ultrasound-assisted UV photolysis treatment and its visible light photocatalysis activity. *Nanotechnol. Rev.* **2023**, *12*, 20220503. [[CrossRef](#)]
10. Nasar, A.; Mashkoo, F. Application of polyaniline-based adsorbents for dye removal from water and wastewater—A review. *Environ. Sci. Pollut. Res.* **2019**, *26*, 5333–5356. [[CrossRef](#)] [[PubMed](#)]
11. Saeed, M.; Muneer, M.; Haq, A.; Akram, N. Photocatalysis: An effective tool for photodegradation of dyes—A review. *Environ. Sci. Pollut. Res.* **2022**, *29*, 293–311. [[CrossRef](#)] [[PubMed](#)]
12. Jonathan, R.; Rehman, S.U.; Cao, F.; Xu, H.; Ma, X.; Wang, J.W.; Liu, Y.F.; Niu, Y.H.; Jian, X.; Mahmood, N. Low-cost and large-scale preparation of ultrafine TiO₂@C hybrids for high-performance degradation of methyl orange and formaldehyde under visible light. *Nanotechnol. Rev.* **2023**, *12*, 20220556. [[CrossRef](#)]
13. Deng, F.; Pei, X.; Luo, Y.; Luo, X.; Dionysiou, D.; Wu, S.; Luo, S. Fabrication of Hierarchically Porous Reduced Graphene Oxide/SnIn₄S₈ Composites by a Low-Temperature Co-Precipitation Strategy and Their Excellent Visible-Light Photocatalytic Mineralization Performance. *Catalysts* **2016**, *6*, 113. [[CrossRef](#)]
14. Tekin, D.; Kiziltas, H.; Urgan, H. Kinetic Evaluation of ZnO/TiO₂ Thin Film Photocatalyst in Photocatalytic Degradation of Orange G. *J. Mol. Liq.* **2020**, *306*, 112905. [[CrossRef](#)]
15. Shathy, R.A.; Fahim, S.A.; Sarker, M.; Quddus, M.S.; Moniruzzaman, M.; Masum, S.M.; Molla, M.A.I. Natural Sunlight Driven Photocatalytic Removal of Toxic Textile Dyes in Water Using B-Doped ZnO/TiO₂ Nanocomposites. *Catalysts* **2022**, *12*, 308. [[CrossRef](#)]
16. Ma, T.; Bai, J.; Li, C. Facile Synthesis of g-C₃N₄ Wrapping on One-Dimensional Carbon Fiber as a Composite Photocatalyst to Degrade Organic Pollutants. *Vacuum* **2017**, *145*, 47–54. [[CrossRef](#)]
17. Shi, H.; Zhao, Y.; Fan, J.; Tang, Z. Applied Surface Science Construction of Novel Z-Scheme Flower-like Bi₂S₃/SnIn₄S₈ Heterojunctions with Enhanced Visible Light Photodegradation and Bactericidal Activity. *Appl. Surf. Sci.* **2019**, *465*, 212–222. [[CrossRef](#)]
18. Chen, C.C.; Shaya, J.; Polychronopoulou, K.; Golovko, V.B.; Tesana, S.; Wang, S.Y.; Lu, C.S. Photocatalytic Degradation of Ethiofenarb by a Visible Light-Driven SnIn₄S₈ Photocatalyst. *Nanomaterials* **2021**, *11*, 1–16. [[CrossRef](#)]
19. Yan, T.; Li, L.; Li, G.; Wang, Y.; Hu, W.; Guan, X. Porous SnIn₄S₈ Microspheres in a New Polymorph that Promotes Dyes Degradation under Visible Light Irradiation. *J. Hazard. Mater.* **2011**, *186*, 272–279. [[CrossRef](#)]
20. Wang, J.; Liu, M.; Wang, M.; Wang, Y.; Zhang, A.; Zhao, X.; Zeng, G.; Deng, F. Bandgap Engineering of Hierarchical Network-like SnIn₄S₈ Microspheres through Preparation Temperature for Excellent Photocatalytic Performance and High Stability. *Green Energy Environ.* **2019**, *4*, 264–269. [[CrossRef](#)]
21. Deng, F.; Lu, X.; Zhao, L.; Luo, Y.; Pei, X.; Luo, X.; Luo, S. Facile Low-Temperature Co-Precipitation Method to Synthesize Hierarchical Network-like g-C₃N₄/SnIn₄S₈ with Superior Photocatalytic Performance. *J. Mater. Sci.* **2016**, *51*, 6998–7007. [[CrossRef](#)]
22. Wang, J.; Wang, B.; Zhang, W.; Xiao, Y.; Xu, H.; Liu, Y.; Liu, Z.; Zhang, J.; Jiang, Y. Visible-light-driven double-shell SnIn₄S₈/TiO₂ heterostructure with enhanced photocatalytic activity for MO removal and Cr(VI) cleanup. *Appl. Surf. Sci.* **2022**, *587*, 152867. [[CrossRef](#)]
23. Du, Z.; Cui, C.; Zhang, S.; Xiao, H.; Ren, E.; Guo, R.; Jiang, S. Visible-Light-Driven Photocatalytic Degradation of Rhodamine B Using Bi₂WO₆/GO Deposited on Polyethylene Terephthalate Fabric. *J. Leather Sci. Eng.* **2020**, *2*, 16. [[CrossRef](#)]

24. Chaudhuri, S.; Wu, C.; Motora, K. Highly efficient solar-light-driven self-floatable $\text{WO}_{2.72}/\text{Fe}_3\text{O}_4$ immobilized cellulose nanofiber aerogel/polypropylene Janus membrane for interfacial photocatalysis. *J. Photochem. Photobiol. A Chem.* **2023**, *438*, 114525. [[CrossRef](#)]
25. Lee, J.; Tseng, H.; Wey, M. Excellent dispersion of solar light responsive photocatalyst in the different polymer films for easy recycling and sustainable hydrogen production. *Sol. Energy* **2022**, *231*, 949–957. [[CrossRef](#)]
26. Liu, H.; Gu, H.; Li, G.; Li, N. Fabrication of PAN/Ag/ZnO Microporous Membrane and Examination of Visible Light Photocatalytic Performance. *Fibers Polym.* **2021**, *22*, 306–313. [[CrossRef](#)]
27. Tran, M.; Fu, C.; Chiang, L.; Hsieh, C.; Liu, S.; Juang, R. Immobilization of TiO_2 and TiO_2 -GO hybrids onto the surface of acrylic acid-grafted polymeric membranes for pollutant removal: Analysis of photocatalytic activity. *J. Environ. Chem. Eng.* **2020**, *8*, 104422. [[CrossRef](#)]
28. Alahiane, S.; Sennaoui, A.; Sakr, F.; Dinne, M.; Qourzal, S.; Assabbane, A. Synchronous role of coupled adsorption-photocatalytic degradation of Direct Red 80 with nanocrystalline TiO_2 -coated non-woven fibres materials in a static batch photoreactor. *Groundw. Sustain. Dev.* **2020**, *11*, 100396. [[CrossRef](#)]
29. Parikh, D.V.; Nam, S.; He, Q.L. Evaluation of Three Flame Retardant (FR) Grey Cotton Blend Nonwoven Fabrics Using Micro-Scale Combustion Calorimeter. *J. Fire Sci.* **2012**, *30*, 187–200. [[CrossRef](#)]
30. Lu, Z.; Peng, J.; Song, M.; Liu, Y.; Liu, X.; Huo, P.; Dong, H.; Yuan, S.; Ma, Z.; Han, S. Improved recyclability and selectivity of environment-friendly MFA-based heterojunction imprinted photocatalyst for secondary pollution free tetracycline orientation degradation. *Chem. Eng. J.* **2019**, *360*, 1262–1276. [[CrossRef](#)]
31. Byun, J.; Landfester, K.; Zhang, K. Conjugated Polymer Hydrogel Photocatalysts with Expandable Photoactive Sites in Water. *Chem. Mater.* **2019**, *31*, 3381–3387. [[CrossRef](#)]
32. Stoilova, O.; Manolva, N.; Rashkov, I. Electrospun Poly(Methyl Methacrylate)/ TiO_2 Composites for Photocatalytic Water Treatment. *Polymers* **2021**, *13*, 3923. [[CrossRef](#)]
33. Fu, Z.; Huang, C.; Zhao, X.; Fu, Z. Study on preparation and recovery of magnetic $\text{BiOI}/\text{rGO}/\text{Fe}_3\text{O}_4$ composite photocatalyst. *Results Phys.* **2020**, *16*, 102931.
34. Zainal, Z.; Hui, L.; Hussein, M.; Abdullah, A.; Hamadneh, I. Characterization of TiO_2 -Chitosan/Glass photocatalyst for the removal of a monoazo dye via photodegradation-adsorption process. *J. Hazard. Mater.* **2009**, *164*, 138–145. [[CrossRef](#)] [[PubMed](#)]
35. Wang, X.; Lu, W.; Chen, Y.; Li, N.; Zhu, Z.; Wang, G.; Chen, W. Effective elimination of antibiotics over hot-melt adhesive sheath-core polyester fiber supported graphitic carbon nitride under solar irradiation. *Chem. Eng. J.* **2018**, *335*, 82–93. [[CrossRef](#)]
36. Dao, M.; Nguyen, T.; Le, V.; Hoang, H.; Le, T.; Pham, T.; Nguyen, T.; Akhmadullin, R.; Lee, H.; Tran, H.; et al. Non-woven polyester fabric-supported cuprous oxide/reduced graphene oxide nanocomposite for photocatalytic degradation of methylene blue. *J. Mater. Sci.* **2021**, *56*, 10353–10366. [[CrossRef](#)]
37. Huo, K.; Wang, J.; Zhuang, T.; Zhao, Y.; Gao, B.; Dou, M.; Wang, X.; Fu, Y.; Wang, D.; Ci, L. Facile fabrication of recyclable and macroscopic D-g- C_3N_4 /sodium alginates/non-woven fabric immobilized photocatalysts with enhanced photocatalytic activity and antibacterial performance. *J. Mater. Sci.* **2021**, *56*, 17584–17600. [[CrossRef](#)]
38. Liu, Z.; Cai, X.; Fan, S.; Zhang, Y.; Hu, H.; Huang, Z.; Liang, J.; Qin, Y. Preparation of a stable polyurethane sponge supported Sn-doped ZnO composite via double-template-regulated bionic mineralization for visible-light-driven photocatalytic degradation of tetracycline. *J. Environ. Chem. Eng.* **2021**, *9*, 105541. [[CrossRef](#)]
39. Tian, S.Q.; Chen, Y.Y.; Zhu, Y.F.; Fan, H.J. A Fluorescent Polyurethane with Covalently Cross-Linked Rhodamine Derivatives. *Polymers* **2020**, *12*, 1989. [[CrossRef](#)] [[PubMed](#)]
40. Liu, R.; Chen, Y.; Fan, H. Design, Characterization, Dyeing Properties, and Application of Acid-Dyeable Polyurethane in the Manufacture of Microfiber Synthetic Leather. *Fibers Polym.* **2015**, *16*, 1970–1980. [[CrossRef](#)]
41. Wen, J.; Sun, Z.; Wang, Z.; Fan, H.; Xiang, J.; Chen, Y.; Yan, J.; Ning, J. Biomimetic Construction of Three-Dimensional Superhydrophobic Microfiber Nonwoven Fabric. *Colloids Surf. A Physicochem. Eng. Asp.* **2021**, *612*, 125990. [[CrossRef](#)]
42. Li, J.; Cui, M.; Wen, J.; Chen, Y.; Shi, B.; Fan, H.; Xiang, J. Leather-like Hierarchical Porous Composites with Outstanding Electromagnetic Interference Shielding Effectiveness and Durability. *Compos. Part B Eng.* **2021**, *225*, 109272. [[CrossRef](#)]
43. Cui, M.; Li, J.; Gao, Q.; Xiang, J.; Chen, Y.; Yan, J.; Fan, H. A Novel Strategy to Fabricate Nylon 6 Based Flame Retardant Microfiber Nonwoven Fabric with Durability. *Colloids Surf. A Physicochem. Eng. Asp.* **2022**, *641*, 128482. [[CrossRef](#)]
44. Al-Etaibi, A.M.; El-Asasery, M.A. Microwave-Assisted Synthesis of Azo Disperse Dyes for Dyeing Polyester Fabrics: Our Contributions over the Past Decade. *Polymers* **2022**, *14*, 1703. [[CrossRef](#)]
45. Imoisili, P.E.; Jen, T.C. Microwave-assisted sol-gel template-free synthesis and characterization of silica nanoparticles obtained from South African coal fly ash. *Nanotechnol. Rev.* **2022**, *11*, 3042–3052. [[CrossRef](#)]
46. Chumha, N.; Pudkon, W.; Chachvalvutikul, A.; Luangwanta, T.; Randorn, C.; Inceesungvorn, B.; Ngamjarurojana, A.; Kaowphong, S. Photocatalytic Activity of CuInS_2 Nanoparticles Synthesized via a Simple and Rapid Microwave Heating Process. *Mater. Res. Express* **2020**, *7*, 015074. [[CrossRef](#)]
47. Li, S.; Xia, X.; Vogt, B.D. Microwave-Enabled Size Control of Iron Oxide Nanoparticles on Reduced Graphene Oxide. *Langmuir* **2021**, *37*, 11131–11141. [[CrossRef](#)]
48. Wang, Z.; Zhao, J.; Gao, Q.; Luo, H.; Fan, H.; Xiang, J.; Chen, Y. Urchin-like SnIn_4S_8 Photocatalyst Synthesized via Microwave Assisted Method with Durable Photocatalytic Performance under Visible Light. *Chem. Phys. Lett.* **2023**, *817*, 140409. [[CrossRef](#)]

49. Cui, M.; Li, J.; Chen, X.; Hong, W.; Chen, Y.; Xiang, J.; Yan, J.; Fan, H. A halogen-free, flame retardant, waterborne polyurethane coating based on the synergistic effect of phosphorus and silicon. *Prog. Org. Coat.* **2021**, *158*, 106359. [[CrossRef](#)]
50. Xu, H.; Dai, J.; Fang, K.; Guo, Y.; Chen, W.; Liu, X.; Zhang, L.; Li, R.; Liu, D.; Xie, R. BiOI/PPy/cotton photocatalytic fabric for efficient organic dye contaminant degradation and self-cleaning application. *Colloids Surf. A Physicochem. Eng. Asp.* **2023**, *674*, 131862. [[CrossRef](#)]
51. Du, Z.; Cheng, C.; Tan, L.; Lan, J.; Jiang, S.; Zhao, L.; Guo, R. Enhanced Photocatalytic Activity of Bi₂WO₆/TiO₂ Composite Coated Polyester Fabric under Visible Light Irradiation. *Appl. Surf. Sci.* **2018**, *435*, 626–634. [[CrossRef](#)]
52. Abdal-Hay, A.; Makhlouf, A.; Khalil, K. Novel, Facile, Single-Step Technique of Polymer/TiO₂ Nanofiber Composites Membrane for Photodegradation of Methylene Blue. *ACS Appl. Mater. Interfaces* **2015**, *7*, 13329–13341. [[CrossRef](#)] [[PubMed](#)]

Disclaimer/Publisher's Note: The statements, opinions and data contained in all publications are solely those of the individual author(s) and contributor(s) and not of MDPI and/or the editor(s). MDPI and/or the editor(s) disclaim responsibility for any injury to people or property resulting from any ideas, methods, instructions or products referred to in the content.